AUT Journal of Mechanical Engineering

AUT J. Mech. Eng., 8(3) (2024) 241-256
DOI: 10.22060/ajme.2024.23103.6102

Prediction of Running-in Behavior for Point Contacts under Mixed Lubrication

Sahar Ghatrehsamani, Amir Arsalan Hemmasian, Ali Babasafari Zamani, Saleh Akbarzadeh*

Department of Mechanical Engineering, Isfahan University of Technology, Isfahan, Iran

ABSTRACT: Tribology concentrates on wear, lubrication, and friction of interacting surfaces in relative motion. Wear, which is the major reason of material dissipation, evolves in three separate stages: severe wear, steady-state, and running-in. Running-in has an important role in the loss of material performance and this process inducts the progress of the key tribological parameters. Hence, the running-in behaviour of a tribocomponent experiencing point contact in a mixed lubrication regime is inquired both experimentally and theoretically. The transient coefficient of the wear pending the running-in is predicted by using the continuum damage mechanics approach. Predictions involve the use of the load-sharing implication, taking into account the contribution of the asperities and the lubricant. The experimental work entails dynasties of pin-on-disk tests. Comparisons of the theoretical prediction and experimental tests of friction coefficient and wear coefficient are found to be in good agreement. In cases in which continuum damage mechanics— which computes the possibility that an asperity creates a wear particle and uses this data to infer a phrase for the coefficient of the wear— can forestall the volume of the wear with an error of less than 30%.

Review History:

Received: Apr. 16, 2024
Revised: Jul. 26, 2024
Accepted: Sep. 10, 2024
Available Online: Sep. 17, 2024

Keywords:

Running-in
Mixed Lubrication
Point Contact
Surface Roughness
Continuum Damage Mechanics (CDM)

1- Introduction

Running-in is commonly referred to as the process during which the interfacial characteristics of two mating surfaces in sliding contact experience time-dependent variation. It occurs during the initial operation of tribocomponents, when the surfaces are pristine. During running-in, the lubricant film thickness, wear coefficient, and friction coefficient experience drastic and time-dependent changes. As the running-in course progresses, the component of the load carried by the roughnesses reduces provided, simultaneously, the lubricant becomes more active in carrying the load.

Fig. 1 shows a typical Stribeck curve with three different lubrication regimes. The horizontal axis is the Hersey number, a function of the lubricant viscosity, speed, and load. The running-in period affects the Stribeck curve since many surface asperities deform and detach and create wear particles [1]. This polishing action associated with the asperities of the surface predominantly occurs in the mixed lubrication regime.

In the mixed lubrication regime, the total load is carried by the lubricant film as well as the asperities [3]:

$$F_n = F_{Roughness} + F_{Lubricant}\ ,\ \frac{1}{\gamma_1}+\frac{1}{\gamma_2}=1 \qquad (1)$$

In Eq. 1, is the total load, is the load carried by the lubricant layer, and is the load carried by roughness. The scaling factors $\gamma_1 = \frac{F_n}{F_R}$ and $\gamma_1 = \frac{F_n}{F_L}$ express the ratio of the total load to the load carried by the roughness and fluid film, respectively.

In 1991, Hu et al. [4] studied the dynamic behaviour of a lubricated sliding wear system during running-in. Later, Lugt et al. [5] investigated the effect of the roughness of the surface on the lubricant layer build-up capability, the friction specifications of surfaces of the rolling bearing, and running-in in a mixed lubrication regime. Horng et al. [6] evaluated wear in lubricated contact and investigated the critical local temperature and frictional energy. They showed that friction power intensity directly correlates to the surface asperity height and roughness pattern. They also investigated factors influencing the wear resistance of rough surfaces, including specific film thickness, surface pitting, frictional heating, and contact temperature [7]. Nogueira et al. [8] proposed a model for anticipating the coefficient of friction in the mixed lubrication regime during running-in. Horng et al. [9] investigated the contact parameters between mating surfaces during the running-in process and showed that contact width and real contact area substantially increased during the running-in process. Akbarzadeh and Khonsari [10-12] studied the effect of operating manners such as initial roughness, speed, and applied load pending running-in on EHL line contact and observed that corresponding to each

*Corresponding author's email: s.akbarzadeh@iut.ac.ir

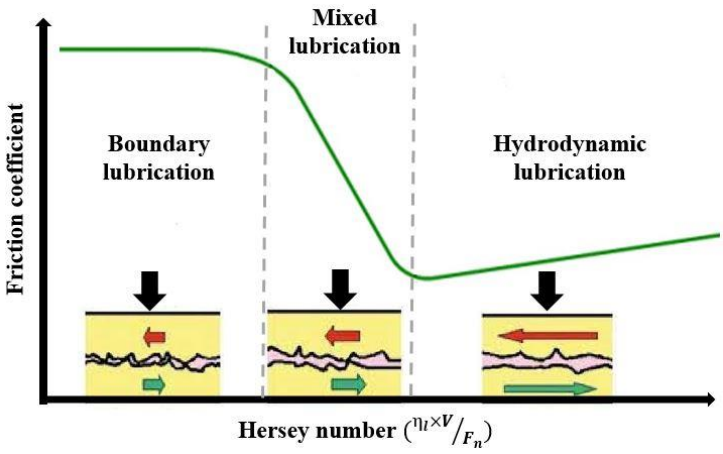

Fig. 1. Different lubrication regimes (Stribeck curve) (reproduced from [2])

applied load, there exists a value for sliding speed that results in a minimum arithmetic average of asperity heights at the end of the running-in period. Sudeep et al. [13] studied the performance of wear, contact fatigue, lubrication, vibration, friction, and noise of lubricated rolling/sliding centralized contacts in attendance of textures of the surface.

Subsequently, Mehdizadeh et al. [14] experimentally investigated the effect of initial surface roughness, running-in speed, and running-in load on weight loss and steady-state friction coefficient. Akbarzadeh et al. [15] conducted multiple tests to check the effects of nanoparticles on the running-in operating conditions and showed that copper and zinc oxide show the foremost efficiency compared to the other lubricants, which reduces the friction coefficient and weight loss up to about 50 %.

Albers and Reichert [16] applied a finite element approach in conjunction with the Archard law to investigate the effect of the roughness of the surface and manufacturing process on the running-in wear depth in the mixed-lubrication regime. Akchurin et al. [17] developed a model based on a critical Von Mises stress and a geometrical boundary condition to predict the formation of wear particles and running-in behaviour in the mixed lubricated contact. Zhang et al. [18] proposed a numerical approach for predicting the evolutions of wear profiles during running-in under mixed lubrication conditions. The results showed that the operating condition in which small wear particles are detached from the contacting surfaces helps decrease the wear rate and friction coefficient and leads to better steady-state performance.

Kragelskii [19] postulated that the formation of a wear particle is an outcome of the fatigue process and that the coefficient of the wear is relevant to the number of cycles needed to form a wear particle. Bhattacharya and Ellingwood [20] developed a model based on the continuum damage mechanics (CDM) wherein the damage parameter was computed in every cycle under fatigue loading. In this project, a numerical model is presented to consider the effect of surface roughness in point-contact mix lubrication in during running-in. Similar to the authors' approach for the behaviour of unlubricated contact during the steady-state and running-in period. Beheshti and Khonsari [21] and Ghatrehsamani and Akbarzadeh [22] used the CDM method for predicting the coefficient of wear for dry contact during steady-state. Beheshti and Khonsari [23] and Samadani and Akbarzadeh [24] used this procedure to forestall the wear coefficient for elastohydrodynamic lubricated contact during steady-state. Ghatrehsamani et al. [25-27] studied the behaviour of unlubricated contact during the running-in period. They predicted friction coefficient, wear rate, and wear coefficient by applying CDM model and experimentally investigated the relation between wear particle size and subsurface stresses in dry sliding contacts. They showed that there is a correlation between the size of the individual particles and the location where the maximum subsurface shear stress occurs. Following that, Salehi et al. [28, 29] developed the applicability of the CDM method for distinguishing wear coefficient in variable loading and speeds.

Nanofluids (NFs) are a new topic of fluids that are used in many industrial applications [30]. In the last two decades, the research on nanotechnology has grown significantly, researchers have conducted a lot of research on this subject in different fields and their irreplaceable role in equipment, lubrication, and heat transfer are significant. Among others, Hemmat Esfe et al. [31-33] investigated the rheological behaviour of hybrid nano lubricants (HNLs) with different composition ratios in a base oil. The goal of the comparison is to determine the HNL with the best lubrication performance at the start of the vehicle and the experimental results of this study introduced the optimal nano polishing to the craft. Also they have evaluated [34] four different models (2FI, quadratic, cubic, and quartic models) for the behaviour of hybrid nanofluid (HNF) based on SAE40 oil using response surface methodology (RSM). Statistical findings show that the quartic model has double accuracy in presenting the HNF properties compared to other models. The viscosity of NF gradually decreases with the increase in temperature and

Table 1. Results of the curve-fit equation for the dimensionless central film thickness and the simulation

Input					$\bar{h}_c$		Error
$\bar{\sigma}_q$ ($\times 10^{-5}$)	G_L ($\times 10^{3}$)	$\overline{F_n}$ ($\times 10^{-4}$)	$\bar{p}_m$ ($\times 10^{-2}$)	$\bar{v}$ ($\times 10^{-11}$)	Simulation ($\times 10^{-5}$)	Curve-fit ($\times 10^{-5}$)	%
$0 \le \bar{\sigma}_q \le 5$	4.5	1	1	1	$1.7 \le \bar{h}_c \le 2.6$	$1.7 \le \bar{h}_c \le 2.5$	$0.2 \le E \le 5.3$
2	$2.5 \le G_L \le 7.5$	1	1	1	$2.2 \le \bar{h}_c \le 2.6$	$2.1 \le \bar{h}_c \le 2.4$	$4.0 \le E \le 5.7$
2	4.5	$2.5 \le \overline{F_n} \le 7.5$	1	1	$1.6 \le \bar{h}_c \le 2.7$	$1.4 \le \bar{h}_c \le 2.6$	$1.1 \le E \le 4.9$
2	4.5	1	$0.5 \le \bar{p}_m \le 3$	1	$2.3 \le \bar{h}_c \le 2.5$	$0.2 \le \bar{h}_c \le 3.1$	$0.5 \le E \le 0.6$
2	4.5	1	1	$0.1 \le \bar{v} \le 10$	$3.4 \le \bar{h}_c \le 9.0$	$3.4 \le \bar{h}_c \le 9.1$	$0.8 \le E \le 7.4$

gradually increases with the increase in SVF [35].

During running-in, the wear and friction between two rough surfaces substantially change. Therefore, initial surface roughness and lubricant between contact surfaces play an important role in decreasing surface damage during running-in. The current work aims to predict the wear coefficient with CDM method in the mixed lubricated contact during running-in on the basis of the load-sharing implication. Finally, the anticipated results are checked with the experimental results designed in during running-in to demonstrate the efficiency of the present procedure.

2- Theory

This part presents the formulation which is used to predict the friction coefficient and the wear coefficient.

2- 1- Friction coefficient

The pressure distribution for the mixed lubricated point contact is governed by the modified Reynolds equation given below (Eq. 2) [36]:

$$\frac{\partial}{\partial x}\left(\varnothing_x \frac{\rho_l h_l^3}{12\eta_l}\frac{\partial P_h}{\partial x}\right)+\frac{\partial}{\partial y}\left(\varnothing_y \frac{\rho_l h_l^3}{12\eta_l}\frac{\partial P_h}{\partial y}\right)=v\frac{\partial(\rho_l h_T)}{\partial x} \quad (2)$$

where is the film thickness equal to the distance between the midline height of the roughness of the two surfaces (m), is the fluid viscosity (Pa.s), is the fluid density (kg/m^3), is the sliding velocity (m/s), is the pressure flow factor in the direction, is pressure flow factor in the direction $\varnothing_x = \varnothing_y = 1-0.9e^{-0.56(\bar{h}_l/\bar{\sigma}_q)}$, is average pressure (Pa), and is the mean gap between the two surfaces (m).

Masjedi and Khonsari [37] developed formulas for predicting the layer thickness of lubricant and roughness load proportion for mixed lubrication point contact by solving the governing equations for various input data. These formulas are functions of dimensionless parameters of , , , and . Thus, a general form of film thickness has been chosen for performing the regression analysis (Eq. 3).

$$(\overline{h_l}) = c_1(\overline{F_n})^{(c_2 k_p^{(m_1)})} c_3 \overline{v}^{(c_4 k_p^{(m_2)})} c_5 G_L^{(c_6 k_p^{(m_3)})(1+c_7 e^{(c_8 k_p)})} \quad (3)$$

where to and to are known constants (dimensionless) to be determined and these dimensionless parameters are dimensionless film thickness $\overline{h_l} = h_l / R$ where is film thickness (m), elliptical parameter $k_p = D_x / D_y = 1$ where and contact diameter in and direction (m), dimensionless load $\overline{F_n} = F_n / ER^2$ where is applied load to the surface (N), is the modulus of elasticity (Pa), and is the effective radius of curvature (m), dimensionless speed $\overline{v} = v\eta_0 / ER$ where is sliding speed (m/s) and is the viscosity at ambient temperature (Pa.s), dimensionless hardness $\overline{p}_m = p_m / E$ where is material flow pressure (Hardness) (Pa), dimensionless material number $G_l = \alpha_{EHL} E$ where is a pressure-viscosity coefficient (m^2/N), and dimensionless surface roughness $\overline{\sigma}_q = \sigma_q / R$ where is surface roughness (m).

To compute the friction coefficient, it is necessary to compute the thickness of the central layer of the lubricant and the roughness load proportion. In Eq. 3, the limited area of input parameters selected for simulation are

$0 \le \bar{\sigma}_q \le 5\times10^{-5}, 1.5\times10^{-7} \le \overline{F_n} \le 2.5\times10^{-4}, 1\times10^{-12} \le \bar{v} \le 2.5\times10^{-10},$
$2500 \le G_L \le 7500, 0.005 \le \bar{p}_m \le 0.03, 1 \le k_p \le 8.$

After analyzing the results of about a hundred simulations, the input-limited area is shown. For example, some results are shown in Table 1. To obtain each curve-fit equation, a suitable shape must be considered. The best curve-fit equations for the dimensionless central layer thickness are gained as Eq. 4 [37].

$$(\overline{h_c})_{smooth} = \frac{(h_c)_{smooth}}{R} = 3.672(\overline{F_n})^{(-0.045k_p^{0.18})} \overline{v}^{(0.663k_p^{0.18})} G_L^{(0.502k_p^{0.064})(1-0.573e^{(-0.74k_p)})} \quad (4)$$

Considering surface roughness, the relationship between the central film thickness (Eq. 5) as well as the roughness

load proportion, L_a, is gained as Eq. 6 [37].

$$\overline{h}_c = \frac{h_c}{R} = \left(\overline{h}_c\right)_{smooth} \times \left(1 + 0.025\overline{\sigma}_q^{\,1.248}\overline{p}_m^{\,0.119}\overline{F_n}^{-0.133}\overline{v}^{-0.884}G_L^{\,-0.977}k_p^{\,-0.081}\right) \quad (5)$$

$$L_a = 10\overline{F_T}^{-0.083}\overline{v}^{0.143}G_L^{\,-0.314}{}^{0.501} \times \left(\ln\left(1+\overline{\sigma}_q^{\,4.689}\overline{p}_m^{\,0.509}\overline{F_n}^{-0.501}\overline{v}^{-2.9}G_L^{\,-2.870}\right)\right) \quad (6)$$

The load endured by asperities is resolved using the following (Eq. 7) [3]:

$$F_R = \frac{L_a}{100} \times F_n \quad (7)$$

Also, the total friction force (Eq. 8) is the sum of the two components of the asperity friction force and hydrodynamic friction force . Therefore, the total friction coefficient for the lubricated contact is calculated from Eq. 9 [37].

$$F_f = F_{f,L} + F_{f,R} \rightarrow \begin{cases} F_{f,R} = 0.12 \times F_R \\ F_{f,L} = A \times \tau_h \times \left[1 - exp\left(-\eta_l\left(\frac{v}{h_c}\right)/\tau_h\right)\right] \end{cases} \quad (8)$$

$$\mu = \frac{F_{f,L} + F_{f,R}}{F_n}$$
$$\tau_h = \Lambda_h P_h \left[1 - \frac{L_a}{100}\right] \quad (9)$$
$$\eta_l = \eta_0 \times \left(\frac{\eta_\infty}{\eta_0}\right)^{\left[1-\left(1+\frac{P_h}{C_P}\right)^{Z_p}\right]}$$

Where

$$\eta_\infty = 6.53 \times 10^{(-5)}$$

$$Z_p = [7.81(H_{40} - H_{100})]^{1.5} \times F_{40} \quad (10)$$

Where

$$H_{40} = \log\left(\log(\eta_{40}) + 1.2\right)$$

$$H_{100} = \log\left(\log(\eta_{100}) + 1.2\right)$$

$$F_{40} = 0.885 - 0.864H_{40}$$

$$\alpha_{EHL} = Z_p\left(5.1 \times 10^{-9} \times \left(\ln\eta_0 + 9.67\right)\right) \quad (11)$$

In these relationships is the limiting shear stress, is the limiting shear stress coefficient, is the viscosity at ambient temperature, A is the area of contact, and is the pressure-viscosity index, which can also be calculated from Eq. 10 and 11. and are the oil viscosities at 40 and 100 ° C, respectively [38].

2- 2- Wear coefficient

The wear volume is predicted using the Archard equation (Eq. 12) [39]. In this equation, is the specific heat capacity, is the sliding distance, is the applied load, is the coefficient of the wear, and is the volume of the wear. Also Kragelskii [19] demonstrated that the coefficient of wear () is relevant to the number of cycles needed () to form a wear particle $\frac{1}{3l_c}$.

$$V_{wl} = K_l \frac{F_n\, S_l}{p_m} \rightarrow K_l = \frac{1}{3l_c} \quad (12)$$

In the CDM procedure, a fracture occurs when the accumulated damage (D_l) reaches the critical damage value ($D_{cr.}$). During each cycle, additional damage occurs inside the material. The damage parameter can be quantified by $D_l = 1 - \frac{E_D}{E}$ in which the modulus of elasticity for the damaged material is $E_D = E(1 - D_l)$ and the modulus of elasticity for the undamaged material is $E = \frac{\sigma}{\varepsilon}$. Eq. 13 gives the hysteresis loop for isotropic damage growth in a deformed object $D_{l_{(l_c)}}$.

$$D_{l_{(l_c)}} = 1 - \left(1 - D_{l_{(l_{c-1})}}\right)\frac{\frac{1}{1+1/M_h}\Delta\varepsilon_{o(l_c)}^{1+1/M_h} - \Delta\varepsilon_{l(l_c)}^{1/M_h}\Delta\varepsilon_{o(l_c)} + C_{(l_c)}}{\frac{1}{1+1/M_h}\Delta\varepsilon_{o(l_c)}^{1+1/M_h} - \Delta\varepsilon_{l(l_c))}^{1/M_h}\Delta\varepsilon_{o(l_c)} + C_{(l_c)}} \quad (13)$$

if $\sigma_{max} \geq S_{fl}$
otherwise $D_{l_{(l_c)}} = D_{l_{(l_{c-1})}}$,

where $C_{(l_c)} = \frac{3}{4}\frac{\sigma_f}{B_l} - \frac{\Delta\varepsilon_{o(l_c)}^{1+1/E_l}}{1+1/E_l} + \Delta\varepsilon_{l(l_c)}^{1/E_l}\Delta\varepsilon_{o(l_c)}$. $B_l = 2^{1-\frac{1}{E_l}}M_l$,

represents the cyclic hardening exponent, is the cyclic hardening modulus, is the fatigue limit, and denotes the true failure stress. Damage caused after cycles is equal to Eq. 14:

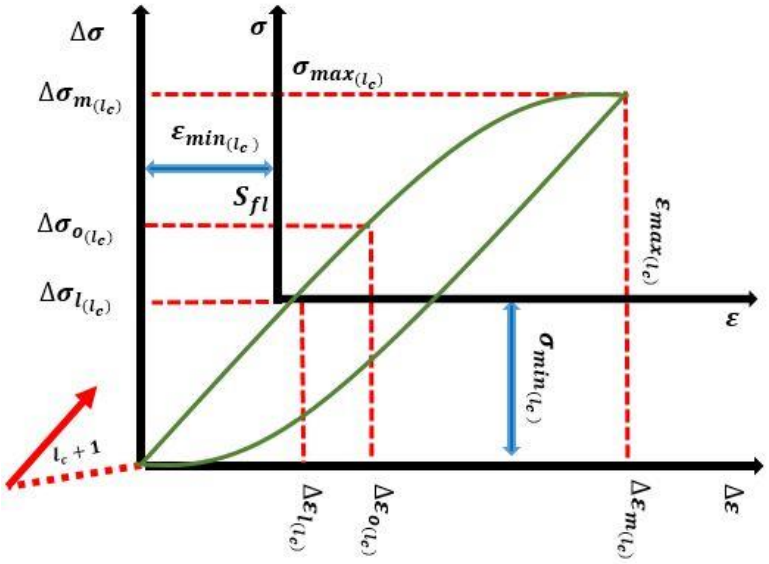

Fig. 2. The solution algorithm of prediction in lubricated contact during the running-in (reproduced from [26])

$$D_{(l_c)} = 1-\left(1-D_0\right)\prod_{k=1}^{l_c} f\left(\varepsilon_k,\alpha\right) \rightarrow \tag{14}$$

$$\alpha = \left\{E, M_l, E_l, S_{fl}, \sigma_f\right\}$$

Where α illustrates material properties and the loading conditions. Considering the controlled strain cycle the strain range, $\Delta\varepsilon_m = \varepsilon_{max} - \varepsilon_{min}$ remains stable. Accordingly, the maximum nominal stress range, $\Delta\sigma_m = \sigma_{max} - \sigma_{min}$ remains stable, and $\Delta\varepsilon_{m(l_c)}$ is obtained in terms of $\Delta\sigma_{m(l_c)}$ and the other plastic strain ranges used in Eq. 15.

$$\Delta\varepsilon_{m(l_c)} = \left(\frac{\Delta\sigma_{m(l_c)}}{B_l\left(1-D_{(l_c-1)}\right)}\right)^{E_l}$$

$$\Delta\varepsilon_{l(l_c)} = \left(\frac{\Delta\sigma_{l(l_c)}}{B_l\left(1-D_{(l_c-1)}\right)}\right)^{E_l} \tag{15}$$

$$\Delta\varepsilon_{o(l_c)} = \left(\frac{\Delta\sigma_{l(l_c)}}{B_l\left(1-D_{(l_c-1)}\right)} + \frac{S_{fl}}{B_l}\right)^{E_l}$$

Where

$$\Delta\sigma_{l(l_c)} = \sigma_{min} = 0 \ , \Delta\sigma_{m(l_c)} = \sigma_{max} - \sigma_{min} = \sigma_{max} = \tau_l = \mu p_m$$

The number of cycles, l_c, needed for the damage parameter to attain its critical value and the unloading part of the hysteresis loop are schematically displayed in Fig. 2. Similar to fretting fatigue, these cracks are imputed to the frictional force. Consequently, shear stress is computed using $\tau_l = \mu p_m$ and then the coefficient of the wear and the rate of wear can be predicted. Also, the flowchart of the solution is shown in Fig. 3.

3- Experimental setup

This part renders the experimental manner for investigating the applied load effect and the roughness of the surface on the running-in wear in the mixed lubrication contact. Tests are managed using a pin-on-disk rig.

3- 1- Specimen preparation

The pins are built of bearing steel and the disks are built of steel CK45 and ST37. The mechanical properties of the disk, the pin, the CDM parameters, and the lubricant are reported in Table 2. The tests were repeated at least twice to ensure the repeatability of the results.

The CDM parameters are obtained from a simple tensile test by the tensile test device Santam STM-50 in which the

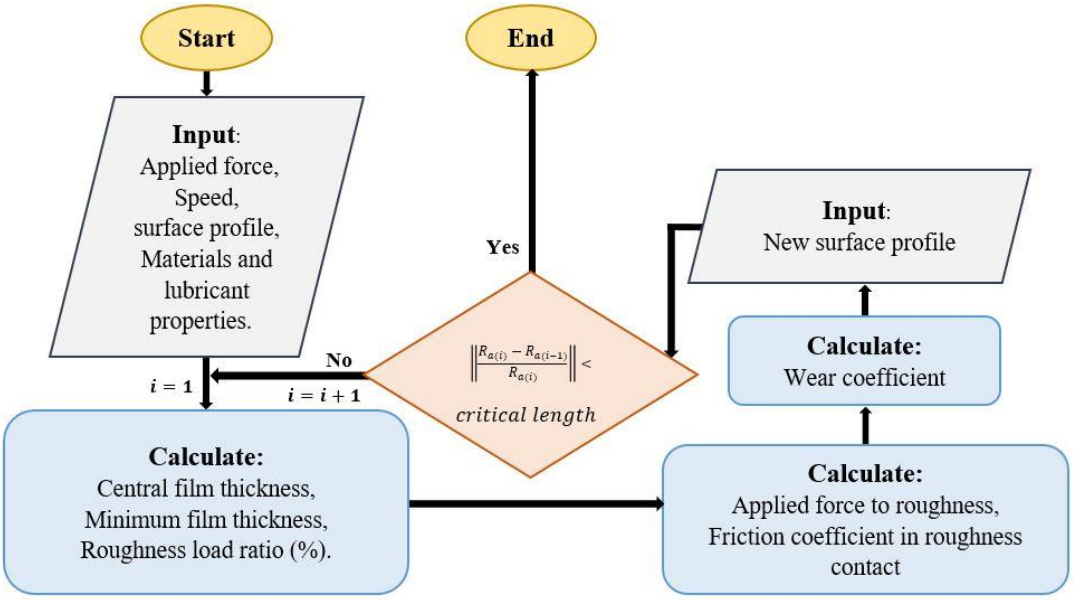

Fig. 3. The solution algorithm of prediction in lubricated contact during the running-in

Table 2. Pin, disk, and lubricant material properties

	Material Properties and the CDM parameters [40]						Lubricant		
	p_m (GPa)	E (GPa)	M_l	ν	D_c	σ_f (GPa)	SAE10		
Pin	8.2	220	-	0.26	-	-	η_0 (Pa.s)	H_{40}	H_{100}
Disk ST37	1.6	195	7.2	0.28	0.42	0.119	0.0259	28	4.9
Disk CK45	2.12	200	7.2	0.29	0.5	0.3			

strain was recorded by extensometer. Also, using the stress-strain curve during loading and using equation $D_l = 1 - \frac{E_D}{E}$, the intermediate of the parameter of the critical damage from ten cycles in a tensile test for CK45 and ST37 was computed.

A series of experiments under constant load but different speeds were conducted to ensure that the tests were performed in the mixed lubrication regime. In the lubricated case, a fixture has been added to the pin-on-disc rig in which the disk is submerged in a lubricant bath. The average value of the friction coefficient was calculated and shown in Fig. 4. It is observed that the coefficient of friction decreases as the speed increases, which is an indication of the mixed lubrication regime.

In Fig 1-Stribeck curve with three different lubrication regimes is shown. The mixed lubrication regime prevails when the speed of the gears is sufficient to create a lubricating film, but its thickness does not provide complete separation of the contact surfaces. Consequently, there is direct contact between the highest roughnesses, which may lead to accelerated performance. Therefore, the amount of friction force and wear rate is significantly lower than boundary lubrication.

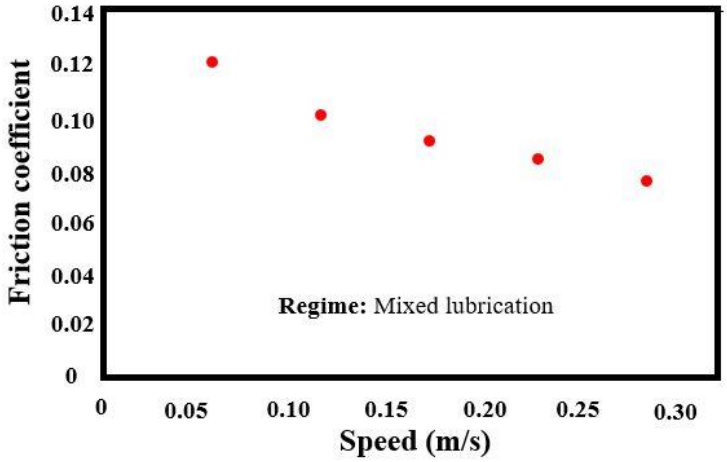

Fig. 4. Test results at different speeds to ensure being in the mixed Lubrication regime

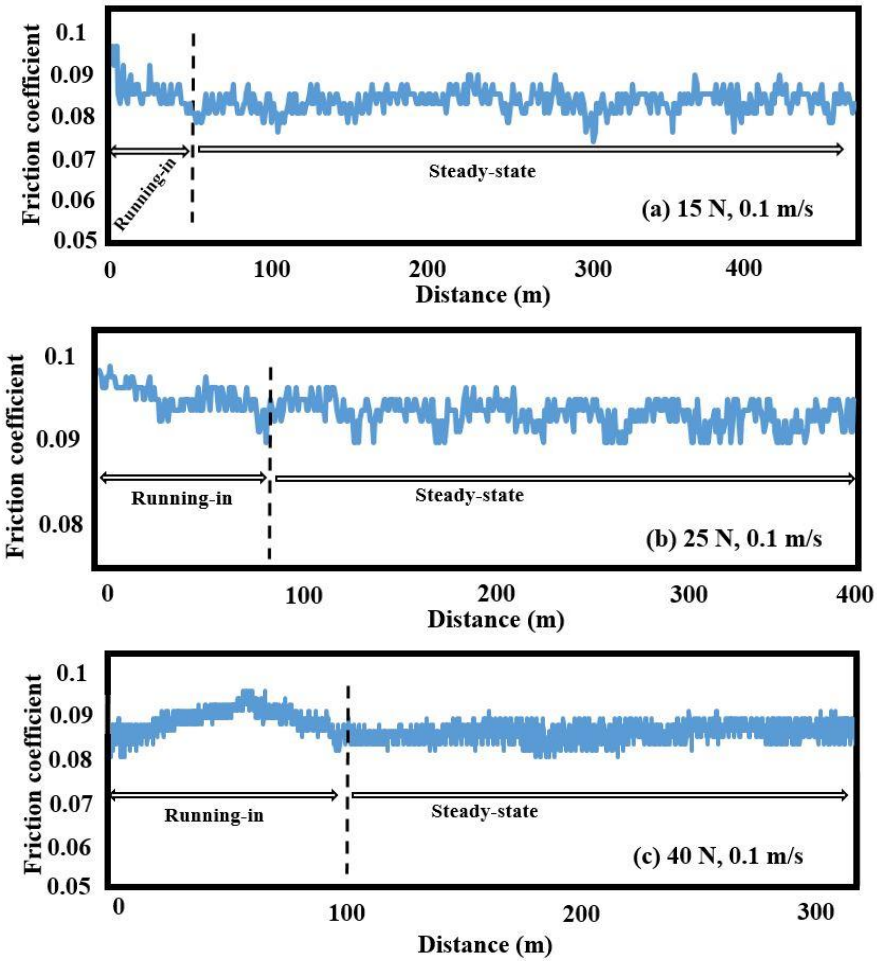

Fig. 5. Wear test and running-in distance determination of CK45 steel disk (a) 15, (b) 25, and (c) 40 N

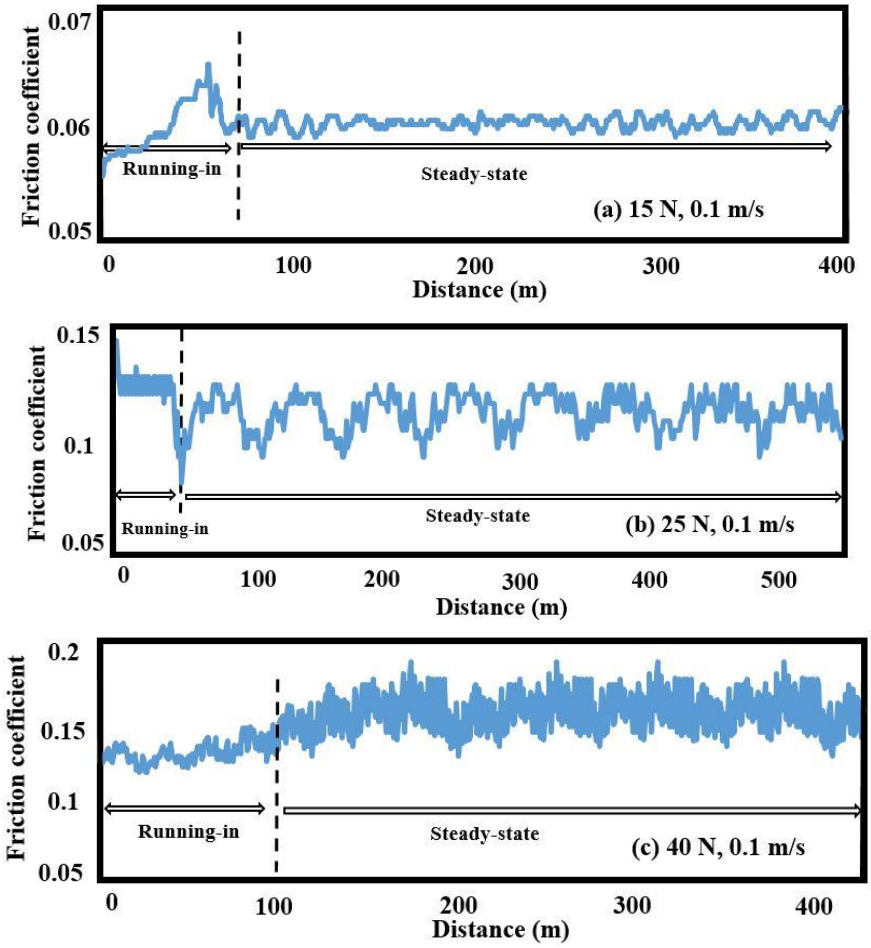

Fig. 6. Wear test and running-in distance determination of ST37 steel disk (a) 15, (b) 25, and (c) 40 N

3- 2- Design of Experiment

In the next step, experiments under a constant speed of 0.1 m/s and different applied loads of 15, 25, and 40 N were conducted to determine the running-in duration. Before each test, the surfaces were polished and the roughness of the surface was measured using a stylus profilometer. The weight of each disk was measured using a digital scale prior to each experiment. A test was first conducted for each operating condition until a steady-state regime was reached to determine the running-in distance. Afterwards, the running-in distance was distributed into five distances and a series of tests were managed under similar operating states, each test was stopped at a determined interval, and the weight loss of the sample and the R_a were measured. For instance, referring to Fig. 5 (a), in the test with Ck45 steel disks at an applied load of 15 N and a sliding speed of 0.1 m/s, the running-in distance is 50 m. Therefore, the running-in interval was distributed into five distances (0-10 m), (0-20 m), (0-30 m), (0-40 m), (0-50 m). In Fig. 5 (a), the variation in the composition of the surface of the disk diminishes the primary friction. The weight loss and R_a were measured in each test. The wear volume of each coated specimen was examined and compared with the results obtained from CDM . Figs. 5 and 6 show the running-in distance for different loads and materials. The friction coefficient behaviour pending running-in is different on the basis of material properties and the applied load. In the case shown in Fig. 6 (a), customarily apperceived in steel-to-steel contact, the primary roughness of the surface brings about a primary increase in the coefficient of friction until the contacting surfaces align, and the coefficient of friction drops.

The behaviour of the coefficient of the friction during running-in in case Fig. 5 (c) is in the exponential shape and owing to the development of the oxide film and the development in the contact geometry. In Fig. 6 (c), generally seen in steel-to-steel contact, the primary roughness of the surface brings about an primary increase in the coefficient of the friction until the surfaces of the contacting align, and the coefficient of the friction drops. In Figs. 5 (a), (b) and Fig. 6 (b), the variation in the composition of the surface of the disk reduces the primary friction.

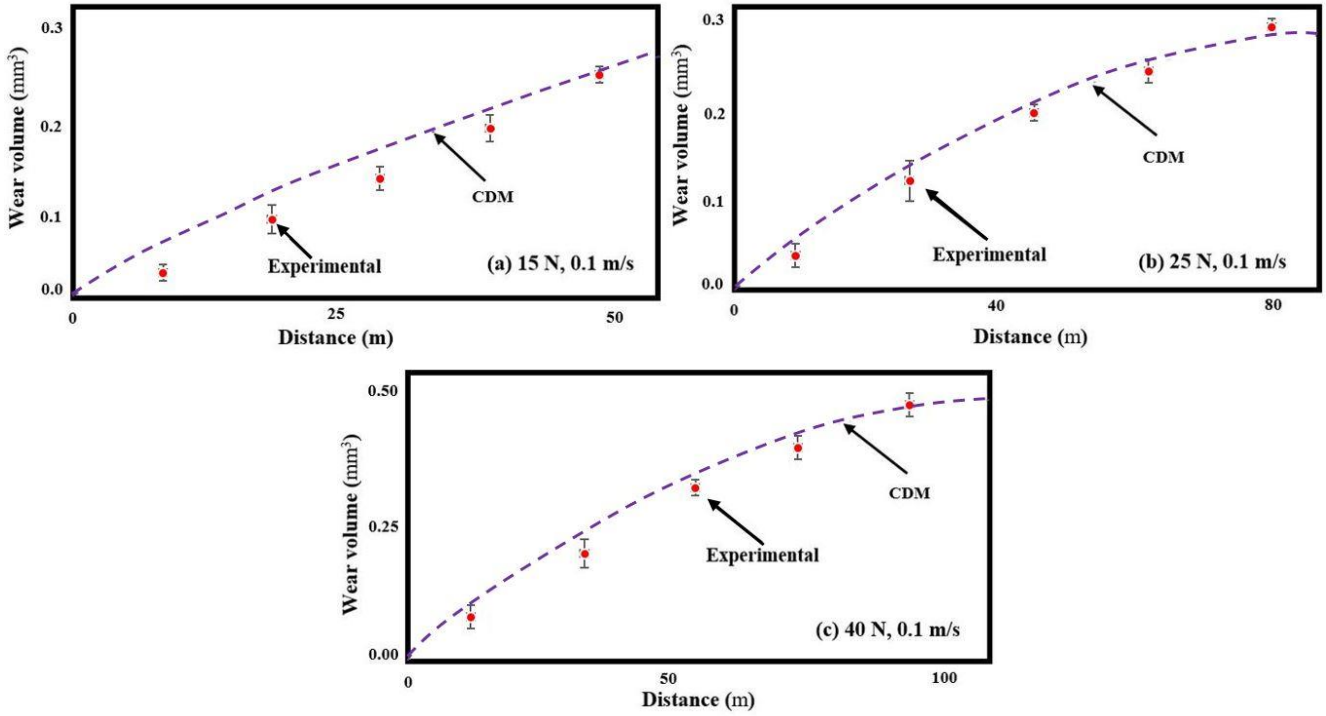

Fig. 7. The wear volume at each step of the running-in period of CK45 steel disk (a) 15, (b) 25, and (c) 40 N

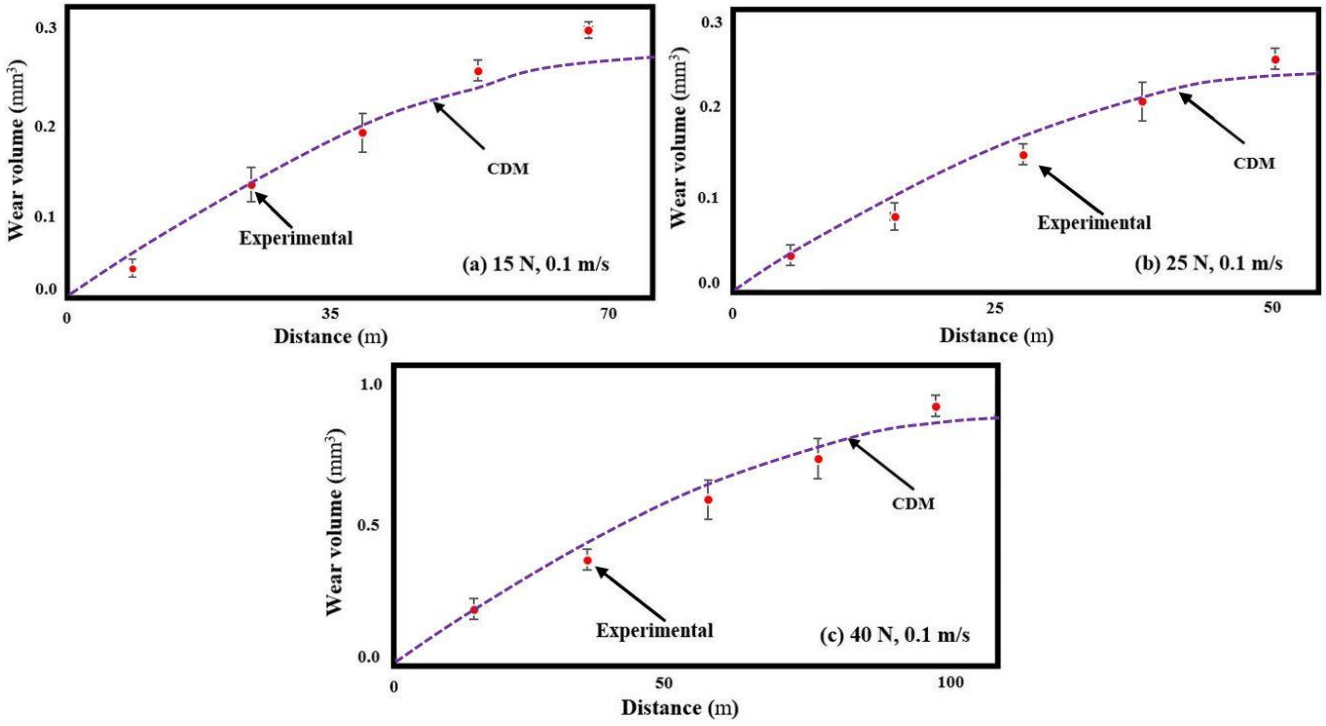

Fig. 8. The wear volume at every stage of the running-in period of ST37 steel disk (a) 15, (b) 25, and (c) 40 N

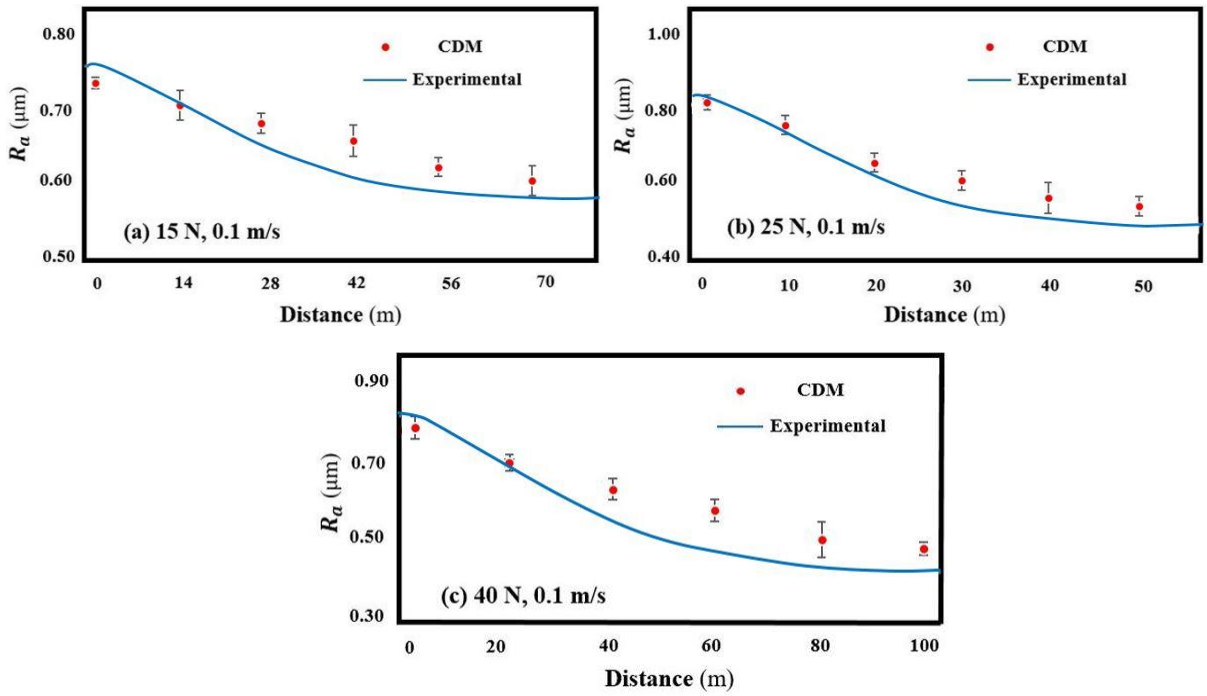

Fig. 9. Ra measurements at each step of the running-in course of ST37 steel disk (a) 15, (b) 25, and (c) 40 N

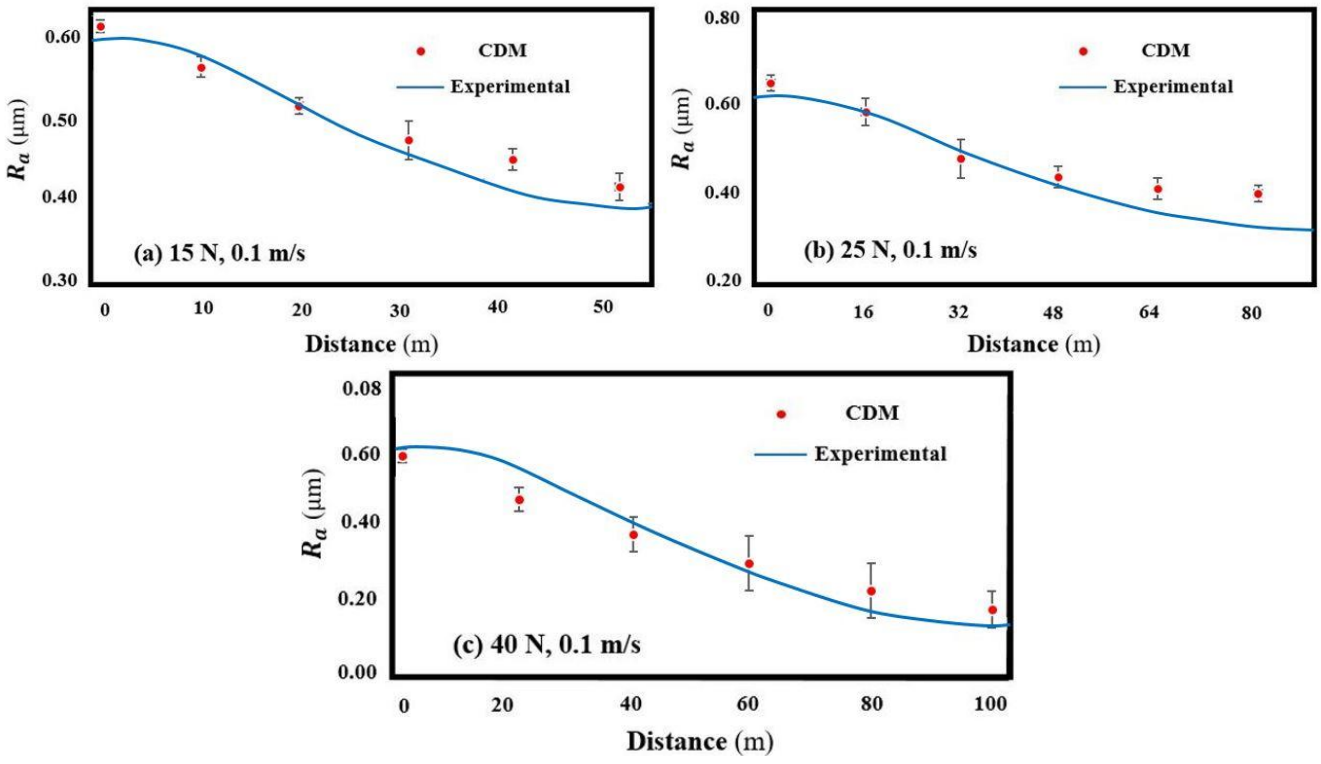

Fig. 10. Ra measurements at each step of the running-in course of CK45 steel disk (a) 15, (b) 25, and (c) 40 N

Table 3. Comparison and analysis of wear volume results

1	2	3	4	5	6	7	8	9
	Material	**Load (N)**	**Mean COF**	**Running-in Distance** (m)	**Weight loss Experimental** (10^{-4} gr)	**Wear volume by Experiment** (mm^3)	**Wear volume CDM** (mm^3)	**Error wear volume (%)**
1	CK45	15	0.086	10	2.30	0.03	0.05	24
				20	8.50	0.11	0.14	21.0
				30	11.70	0.15	0.17	11.7
				40	15.60	0.20	0.21	4.7
				50	20.28	0.26	0.26	0.3
2		25	0.093	32	10.14	0.13	0.15	13.3
3		40	0.090	40	17.16	0.22	0.25	12.0
4	ST37	15	0.062	70	13.40	0.30	0.27	10.0
5		25	0.125	20	6.24	0.08	0.11	27.2
6		40	0.151	60	46.80	0.60	0.70	14.2

4- Results and discussion

Fig. 7 shows the volume of the wear at each stage of the running-in course under loads 15, 25, 40 N at a speed of 0.1m/s for CK45 steel disk and Fig. 8 shows the wear volume for ST37 steel disk. The wear rate is initially high and as the sharp asperities are gradually polished, the wear rate decreases. The operating manners for the running-in course should be attentively opted to improve the steady-state efficiency of the system. This model considers the surface properties and the loading condition and uses these parameters as input and predicts the wear coefficient during running-in. The following graphs and results are drawn using data exchange between MATLAB and Excel.

Figs. 9 and 10 compare experimentally and predicted measured amounts of arithmetic mean roughness at each stage of the running-in course gained for materials CK45 and ST37 under loads of 15 N, 25 N, and 40 N , respectively. As the applied load increases, more roughness experiences contact, resulting in larger plastic deformation and wear depth. This is particularly noticeable in the results of 40 N load on ST37 disk since its hardness is 25% lower than the CK45 disk. It shows that R_a decreases during the running-in period, and the roughness variation stabilizes after the surfaces run in. It is worth noting that the value of surface roughness at the end of running-in plays a main duty in the steady state proficiency of the tribo-system.

Table 3 shows the predicted volume of the wear and wear volume gained from the experimental for both CK45 and ST37 materials at constant speed. Row 1 in the table is the comparison of the measured and predicted volume of the wear for each stage during running-in. The rest of the rows are given for a phase of the transition period where the difference between the predicted and experimental wear volume is maximum. For example, in Row 5, for ST37 in loading 25 N and the first stage of running-in period (20 m), the difference between the predicted and experimental wear volume is 27. 2 percent. In Column 9, as can be seen, the difference between the experimental results and the CDM model is between 0.3-27%.

Table 4 shows a comparison of the measured and predicted arithmetic mean roughness () for both CK45 and ST37 at constant speed at each stage of wear pending running-in. In Table 4, the roughness profile changes are reported for each stage of the running-in period for ST37 at loading 15 N and for CK45 at loading 40 N, and the biggest difference is reported for the rest of the loadings. The error percentage between the initial and final roughness difference (end of running-in period) shows that the difference between experimental and predicted results is not more than % 17. The outcomes illustrate that model can predict Ra and the volume of the wear with passable precision for this condition.

Fig. 11 shows the effect of sliding velocity on the steady-state friction coefficient of ST37 disk under loads of 10 and 30 N. For each applied load, the predicted of coefficient of friction as a function of dimensionless velocity is illustrated. As speed increases, a thicker lubricant layer is formed and

Table 4. Comparison and analysis of R_a results

ST37			CK45		
Load	Distance	R_a Exp.	Load	Distance	R_a Exp.
15	initial	0.737	40	initial	0.600
	14	0.709		20	0.434
	28	0.607		40	0.389
	42	0.650		60	0.301
	56	0.630		80	0.211
	70	0.610		100	0.190
	70	$\Delta R_{a(\text{exp.})}$=0.737-0.610=0.117		100	$\Delta R_{a(\text{exp.})}$=0.600-0.190=0.410
		$\Delta R_{a(\text{model})}$=0.737-0.590=0.147			$\Delta R_{a(\text{model})}$=0.600-0.182=0.418
		Error=17.2 %			Error=1.9 %
25	50	$\Delta R_{a(\text{exp.})}$=0.810-0.541=0.269	25	80	$\Delta R_{a(\text{exp.})}$=0.600-0.410=0.190
		$\Delta R_{a(\text{model})}$=0.810-0.510=0.300			$\Delta R_{a(\text{model})}$=0.600-0.380=0.220
		Error=1.3 %			Error=13.6 %

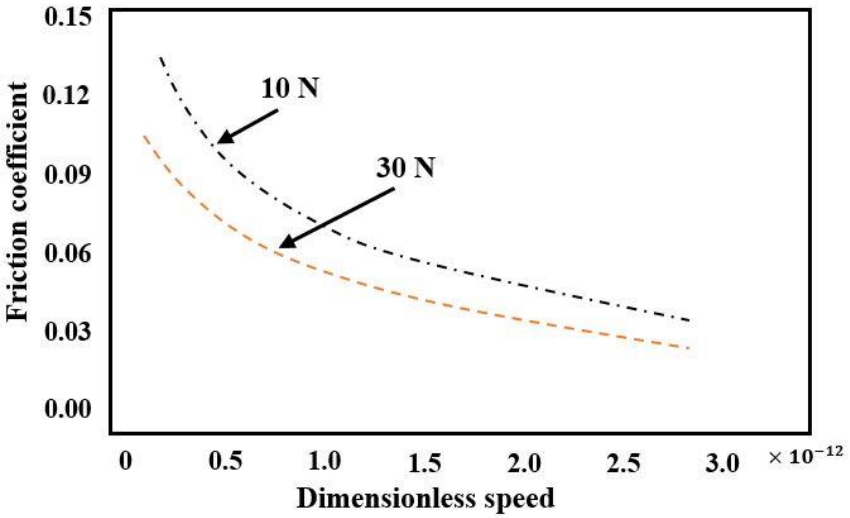

Fig. 11. Effect of sliding velocity on the friction coefficient of ST37 disk

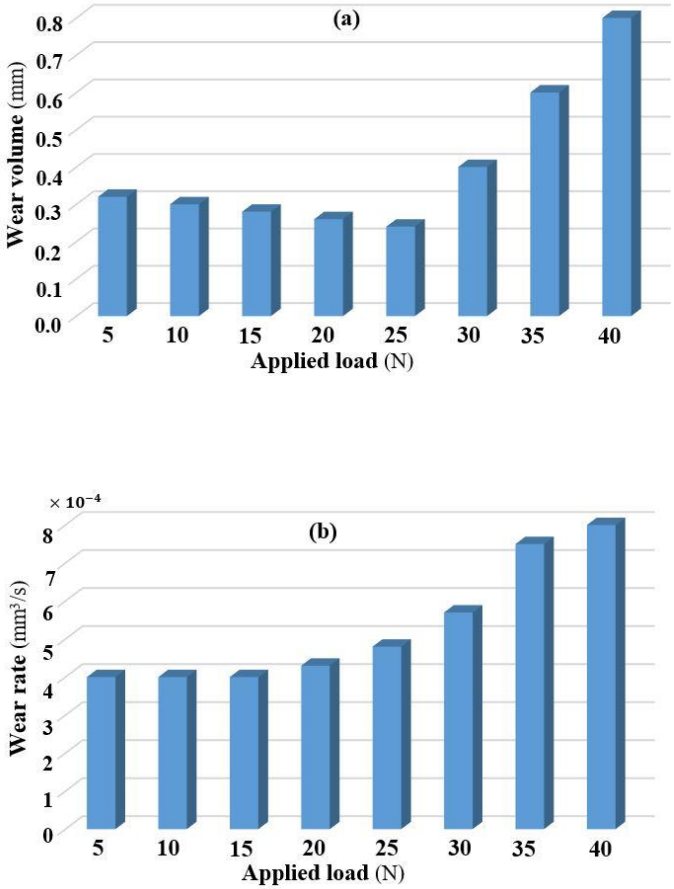

Fig. 12. Comparison of (a) the volume and (b) the rate of the wear under different loading and speed 0.1 m/s

thus less roughness-roughness contact happens and the coefficient of the friction diminishes. At a constant applied speed, increase in the applied load results in lower friction coefficient. These two behaviors are characteristics of mixed lubrication contact.

The CDM method can be used to specify the running-in behaviour, and that the steady-state wear is strongly influenced by the load and speed during the running-in period. Fig. 12 shows an evaluation of the prediction of the volume and rate of the wear gained from simulation from simulation for ST37 materials in each loading and constant speed 0.1 m/s. For example, the coefficient of the friction under a load of 25 N and speed of 0.1 m/s is predicted 0.04, then in the distance of 50 m (at the beginning of the steady-state course) the volume and rate of the wear are predicted 0.24 mm^3 and mm^3/s, respectively. The results show that steady-state performance can be optimized by selecting the pertinent load or speed. Both elasto-hydrodynamic lubrication and metal-to-metal contact occur in mixed lubrication. The load is supported partly by the fluid film and partly by the surface asperities. With the enhancement of applied load, the contact of roughness and the plastic deformation of roughness increase, also the rate of the wear increases.

5- Conclusions

During the running-in period, the lubricant layer thickness can be so small that contact arises at the peaks of surface roughness. This is a transient period wherein both the friction and wear coefficient increase. This paper predicts the friction coefficient using the operating manners, lubricant properties, and surface properties. Then, the point-contact the coefficient of the wear pending the running-in period is predicted by attributing the friction coefficient to CDM model.

Formulas are derived for predicting the central film thickness and the roughness load proportion in point-contact the mixed lubrication of rough surfaces. The rough mixed lubrication model includes a simultaneous solution to the modified Reynolds and surface deformation equations. Regression analyses on the basis of the outcomes from a vast set of simulations are done to gain predictive phases for the film thickness and the roughness load proportion. These formulas are of the form f (, , , and), where the parameters

displayed are dimensionless elliptical parameters, material, load, and velocity, respectively. The predicted results using these formulas are in good agreement with the extensive span of information available in the literature.

The novelty of this paper is in predicting the wear coefficient during running-in for mixed lubrication regime using the CDM model. Two kinds of disks, ST37 and CK45, were tested to corroborate the model. The tests were conducted using a pin-on-disc machine with SAE10 lubricant. . Comparing the results displayed, it is observed that the calculated maximum error in the predicted wear volume and arithmetic mean roughness at each stage running-in are 1% and 5%, respectively. It is shown that the predicted results are fairly close to the experimental data. It is shown that the predicted results are fairly close to the experimental data. Afterwards, the model can supply insight into the running-in behaviour of point-contact problems and reduce extensive experimental testing requirements. Importantly, the model can be used as a guide for selecting the sliding speed or load to achieve the optimum steady-state performance in terms of wear rate or power loss.

6- Nomenclature

Symbol	Description	Symbol	Description
A	Area of contact, (m^2)	S_l	Sliding distance, (m)
C_p	Specific heat capacity, (J/kg.K)	v	Sliding speed, (m/s)
D_l	Damage	$\bar{v}$	Dimensionless speed
$D_{cr.}$	Critical damage	V_{wl}	Wear volume, (m^3)
D_x, D_y	Contact diameter in x and y direction, (m)	Z_p	Pressure-viscosity index
E	Modulus of elasticity (undamaged), (Pa)	α_{EHL}	Pressure-viscosity coefficient, (m^2/N)
E_D	Modulus of elasticity (damaged), (Pa)	γ_1, γ_2	The ratio of total load to the load on the fluid film and roughness
E_l	Cyclic hardening exponent	$\Delta\varepsilon_{ll_c}, \Delta\varepsilon_{ml_c}, \Delta\varepsilon_{ol_c}$	Initial, final plastic, and threshold strain in l_cth cycle
$F_{f,l}$	Hydrodynamic friction force	$\Delta\sigma_{ll_c}, \Delta\sigma_{ml_c}, \Delta\sigma_{ol_c}$	Initial, final plastic, and threshold stress in l_cth cycle, (Pa)
$F_{f,R}$	Roughness friction force		
F_l	Applied load to the fluid film, (N)	η_0	Viscosity at ambient temperature (Pa.s)
F_n	Applied load to the surface, (N)		
$\overline{F_n}$	Dimensionless load	η_{40}, η_{100}	Oil viscosity at 40 and 100˚C, (Pa.s)
F_R	Applied load to the surface roughness, (N)	η_l	Fluid speed, (Pa.s)
G_l	Dimensionless material number	Λ_h	Finite shear stress coefficient
h_c	Centeral film thickness, (m)	μ	Friction coefficient
$\overline{h_c}$	Dimensionless centeral film thickness	ν	Poisson's ratio
h_l	Film thickness, (m)	ρ_l	Fluid density, (kg/m^3)
$\overline{h_l}$	Dimensionless film thickness	σ_f	Failure stress, (Pa)
h_T	Mean gap distance two surfaces, (m)	$\sigma_{max}, \sigma_{min}$	Maximum and minimum normal stress, (MPa)
K_l	Wear friction	σ_q	Surface roughness, (m)
K_p	Elliptical parameter	$\bar{\sigma}_q$	Dimensionless surface roughness
l_c	The number of cycles	τ_h	Limiting shear stress, (Pa)
M_l	Cyclic hardening modulus, (Pa)	τ_l	Finite shear stress
p_m	Material flow pressure (Hardness), (Pa)	$\emptyset_x, \emptyset_y$	Factor of the pressure flow in the x, y direction
$\bar{p}_m$	Dimensionless hardness		
P_h	Average pressure, (Pa)		
R	Effective radius of curvature, (m)		
S_{fl}	Fatigue limit, (Pa)		

References

[1] M.M. Khonsari, S. Ghatrehsamani, S. Akbarzadeh, On the running-in nature of metallic tribo-components: A review, Wear, 474-475 (2021) 203871.

[2] B.J. Hamrock, Fundamentals of Fluid Film Lubrication McGraw-Hill, Inc. Hightstown, NJ, 8520 (1994).

[3] K. Johnson, J. Greenwood, S. Poon, A simple theory of asperity contact in elastohydro-dynamic lubrication, Wear, 19(1) (1972) 91-108.

[4] Y.Z. Hu, N. Li, K. Tønder, A Dynamic System Model for Lubricated Sliding Wear and Running-In, Journal of Tribology, 113(3) (1991) 499-505.

[5] P.M. Lugt, R.W.M. Severt, J. Fogelström, J.H. Tripp, Influence of surface topography on friction, film breakdown and running-in in the mixed lubrication regime, Proceedings of the Institution of Mechanical Engineers, Part J: Journal of Engineering Tribology, 215(6) (2001) 519-533.

[6] J.H. Horng, J.F. Lin, K.Y. Li, Scuffing as evaluated from the viewpoint of surface roughness and friction energy, (1996).

[7] J.H. Horng, True friction power intensity and scuffing in sliding contacts, (1998).

[8] I. Nogueira, A.M. Dias, R. Gras, R. Progri, An experimental model for mixed friction during running-in, Wear, 253(5) (2002) 541-549.

[9] J.H. Horng, M.-L. Len, J.S. Lee, The contact characteristics of rough surfaces in line contact during running-in process, Wear, 253(9-10) (2002) 899-913.

[10] S. Akbarzadeh, M.M. Khonsari, On the Prediction of Running-In Behavior in Mixed-Lubrication Line Contact, Journal of Tribology, 132(3) (2010).

[11] S. Akbarzadeh, M.M. Khonsari, Experimental and theoretical investigation of running-in, Tribology International, 44(2) (2011) 92-100.

[12] S. Akbarzadeh, M.M. Khonsari, On the optimization of running-in operating conditions in applications involving EHL line contact, Wear, 303(1) (2013) 130-137.

[13] U. Sudeep, N. Tandon, R.K. Pandey, Performance of Lubricated Rolling/Sliding Concentrated Contacts With Surface Textures: A Review, Journal of Tribology, 137(3) (2015).

[14] M. Mehdizadeh, S. Akbarzadeh, K. Shams, M.M. Khonsari, Experimental Investigation on the Effect of Operating Conditions on the Running-in Behavior of Lubricated Elliptical Contacts, Tribology Letters, 59(1) (2015) 6.

[15] A. Akbarzadeh, M. Mehdizadeh, S. Akbarzadeh, K. Shams, Effect of nanoparticles on the running-in behavior in lubricated point contact, in, 2015.

[16] A. Albers, S. Reichert, On the influence of surface roughness on the wear behavior in the running-in phase in mixed-lubricated contacts with the finite element method, Wear, 376-377 (2017) 1185-1193.

[17] A. Akchurin, R. Bosman, P.M. Lugt, Generation of wear particles and running-in in mixed lubricated sliding contacts, Tribology International, 110 (2017) 201-208.

[18] Y. Zhang, A. Kovalev, N. Hayashi, K. Nishiura, Y. Meng, Numerical Prediction of Surface Wear and Roughness Parameters During Running-In for Line Contacts Under Mixed Lubrication, Journal of Tribology, 140(6) (2018).

[19] I.V. Kragelsky, V.S. Kombalov, Calculation of value of stable roughness after running-in (elastic contact), Wear, 14(2) (1969) 137-140.

[20] B. Bhattacharya, B. Ellingwood, A new CDM-based approach to structural deterioration, International journal of solids and structures, 36(12) (1999) 1757-1779.

[21] A. Beheshti, M.M. Khonsari, A Thermodynamic Approach for Prediction of Wear Coefficient Under Unlubricated Sliding Condition, Tribology Letters, 38(3) (2010) 347-354.

[22] S. Ghatrehsamani, S. Akbarzadeh, Predicting the wear coefficient and friction coefficient in dry point contact using continuum damage mechanics, Proceedings of the Institution of Mechanical Engineers, Part J: Journal of Engineering Tribology, 233(3) (2018) 447-455.

[23] A. Beheshti, M.M. Khonsari, An engineering approach for the prediction of wear in mixed lubricated contacts, Wear, 308(1) (2013) 121-131.

[24] A. Samadani, S. Akbarzadeh, Experimental and numerical prediction of wear coefficient in non-conformal lubricated rectangular contact using continuum damage mechanics, Surface Topography: Metrology and Properties, 8(2) (2020) 025012.

[25] S. Ghatrehsamani, S. Akbarzadeh, M.M. Khonsari, Experimental and numerical study of the running-in wear coefficient during dry sliding contact, Surface Topography: Metrology and Properties, 9(1) (2021) 015009.

[26] S. Ghatrehsamani, S. Akbarzadeh, M.M. Khonsari, Experimentally verified prediction of friction coefficient and wear rate during running-in dry contact, Tribology International, 170 (2022) 107508.

[27] S. Ghatrehsamani, S. Akbarzadeh, M.M. Khonsari, Relationship between subsurface stress and wear particle size in sliding contacts during running-in, Mechanics Research Communications, 123 (2022) 103891.

[28] S. Salehi, S. Ghatrehsamani, S. Akbarzadeh, M.M. Khonsari, Application of Continuum Damage Mechanics for Prediction of Wear with Provision for Sequential Speed Operation, Tribology Letters, 70(4) (2022) 105.

[29] S. Ghatrehsamani, S. Salehi, S. Akbarzadeh, M.M. Khonsari, On the wear of coated surfaces under variable speed, Tribology International, 187 (2023) 108677.

[30] M.H. Esfe, S.M. Motallebi, S. Alidoust, S.N.H. Tamrabad, D. Toghraie, H. Hatami, Investigation of the effects of various parameters and the evaluation of the optimal rheological of MWCNTs based hybrid nanolubricant and providing an optimal model, Tribology International, 185 (2023) 108534.

[31] M.H. Esfe, H. Hatami, S. Alidoust, D. Toghraie, Can MWCNT (20%)-MgO (80%)/10W40 nano-lubricant be used in industries?(Statistical analysis by focusing on economic factors and rheological behavior for best lubrication conditions), Arabian Journal of Chemistry, 17(1) (2024) 105469.

[32] H. Hatami, R. Tavallaee, M.S. Karajabad, D. Toghraie,

Development of knowledge management in investigating the rheological behavior of SiO2/SAE50 nano-lubricant by response surface methodology (RSM), Tribology International, 187 (2023) 108667.

[33] M.H. Esfe, S. Alidoust, H. Hatami, D. Toghraie, Rheological behavior of 10W40 base oil containing different combinations of MWCNT-Al2O3 nanoparticles and determination of the target nano-lubricant for industrial applications, Micro and Nano Systems Letters, 11(1) (2023) 14.

[34] D. Toghraie, S.N.H. Tamrabad, S. Alidoust, H. Hatami, Obtaining the optimal lubrication conditions by investigating the viscosity of MWCNT (25%)-TiO2 (75%)/oil SAE40 hybrid nanofluid by response surface methodology, Tribology International, 186 (2023) 108585.

[35] M.H. Esfe, R. Tavallaee, D. Toghraie, H. Hatami, Development of knowledge management for viscosity of nanolubricant in hot and cold lubrication conditions, Tribology International, 188 (2023) 108873.

[36] N. Patir, H. Cheng, An average flow model for determining effects of three-dimensional roughness on partial hydrodynamic lubrication, (1978).

[37] M. Masjedi, M. Khonsari, On the effect of surface roughness in point-contact EHL: Formulas for film thickness and asperity load, Tribology International, 82 (2015) 228-244.

[38] C. Roelands, J. Vlugter, H. Waterman, The viscosity-temperature-pressure relationship of lubricating oils and its correlation with chemical constitution, (1963).

[39] J. Archard, Contact and rubbing of flat surfaces, Journal of applied physics, 24(8) (1953) 981-988.

[40] S. Ghatrehsamani, S. Akbarzadeh, M.M. Khonsari, Application of Continuum Damage Mechanics to Predict Wear in Systems Subjected to Variable Loading, Tribology Letters, 69(4) (2021) 163.

HOW TO CITE THIS ARTICLE

S. Ghatrehsamani, A. A. Hemmasian, A. Babasafari Zamani, S. Akbarzadeh, Prediction of Running-in Behavior for Point Contacts under Mixed Lubrication, AUT J. Mech Eng., 8(3) (2024) 241-256.

DOI: 10.22060/ajme.2024.23103.6102